

# A numerical method for computing initial conditions of Lagrangian invariant tori <sup>\*</sup>

Alejandro Luque<sup>†</sup>

Instituto de Ciencias Matemáticas,  
Consejo Superior de Investigaciones Científicas,  
C. Nicolás Cabrera 13-15, 28049 Madrid (Spain).

Jordi Villanueva<sup>‡</sup>

Departament de Matemàtica Aplicada I,  
Universitat Politècnica de Catalunya,  
Av. Diagonal 647, 08028 Barcelona (Spain).

November 10, 2015

## Abstract

We present a numerical method for computing initial conditions of Lagrangian quasi-periodic invariant tori of Hamiltonian systems and symplectic maps. Such initial conditions are found by solving, using the Newton method, a nonlinear system obtained by imposing suitable conditions on the frequency map. The basic tool is a newly developed methodology to perform the frequency analysis of a discrete quasi-periodic signal, allowing to compute frequencies and their derivatives with respect to parameters. Roughly speaking, this method consists in computing suitable weighted averages of the iterates of the signal and using the Richardson extrapolation method. The proposed approach performs with high accuracy at a moderate computational cost. We illustrate the method by considering a discrete FPU model and the vicinity of the point  $L_4$  in a RTBP.

PACS: 02.30.Hq; 02.30.Mv; 02.60.-x; 05.10.-a;

Keywords: Quasi-periodic Lagrangian tori; Hamiltonian systems; Symplectic maps; Derivatives of frequencies.

## 1 Introduction

One of the most remarkable features of Hamiltonian systems and symplectic maps is the huge abundance of quasi-periodic solutions. We refer the interested reader to [2, 7], and references therein, for a wide picture of quasi-periodicity in dynamical systems. A typical way to introduce quasi-periodic solutions is to consider perturbations of integrable systems. The phase space of an integrable Hamiltonian is filled up by *Lagrangian invariant tori carrying quasi-periodic motion* (LIT). The KAM theorem states that most of the LITs of the integrable system, in the sense of the Lebesgue measure, survive to small Hamiltonian perturbations. LITs are also abundant far from integrability, as there are many mechanisms to generate them.

As invariant tori are a fundamental class of stable solutions, computing them is a very relevant problem in the numerical analysis of dynamical systems, and a wide set of algorithms has been developed for this purpose. We summarize some methods for computing LITs and we refer the reader to [15, 28] for a more detailed discussion of the bibliography. LITs have been approximated using methods based on canonical transformations (e.g.

---

<sup>\*</sup>This work has been supported by the Spanish MINECO-FEDER Grants MTM2012-31714, MTM2012-32541 and the Catalan Grants 2014SGR504 and 2014SGR1145. Moreover, A. L. is supported by a postdoctoral position in the ERC Starting Grant 335079.

<sup>†</sup>luque@icmat.es

<sup>‡</sup>jordi.villanueva@upc.edu

28 implementation of KAM proofs [12] or normal forms around an invariant object [13, 21]) or using the Lindstedt-  
 29 Poincaré method [13, 31]. Another approach, valid far from integrability, is to compute a parameterization of the  
 30 LIT as a solution of an invariance equation. This functional equation can be approximated by a finite dimensional  
 31 one, either by discretizing the functional (e.g. [9, 28]) or by truncating the Fourier series of the parameteriza-  
 32 tion (e.g. [3, 17, 29]). Some recent works (e.g. [15, 18]) solve the invariance equation by methods based on the  
 33 parameterization KAM result in [8]. Finally, invariant curves of maps have been computed by interpolating the  
 34 dynamics [22, 31]. This last approach is the closest to our construction, in the sense that it also attempts to compute  
 35 the curve by finding a single point of it.

36 In this paper we compute initial conditions of LITs with prefixed frequencies. To this end we assume that LITs  
 37 can be locally labelled by the frequency vector (e.g. under the Kolmogorov non-degeneracy condition). We can  
 38 identify a point on the LIT by equating the frequency map to the selected frequencies. This leads to a nonlinear  
 39 system of equations with dimension given by the number of degrees of freedom. If we can evaluate the frequency  
 40 map at any point, as well as its derivatives, then this system can be solved by the Newton method.

41 To compute frequencies and their derivatives at a given point, we use an averaging-extrapolation method ap-  
 42 plied to a sample of points of the corresponding orbit. This approach, that was introduced in [30] to compute  
 43 rotation numbers of circle maps, allows computing the frequencies with an error of  $\mathcal{O}(1/N^{p+1})$ , where  $p$  is the  
 44 averaging order and  $N$  the length of the sample. Subsequently, this method was extended to compute derivatives  
 45 of the rotation number [25], to compute quasi-periodic invariant curves of symplectic maps [26] and to perform  
 46 the frequency analysis of an arbitrary quasi-periodic signal [27]. Notice that there are other noteworthy methods  
 47 for the quasi-periodic frequency analysis (e.g. [14, 23]) that could be used also to evaluate the frequency map.

48 Our approach does not require the system to be nearly-integrable nor to be written in a specific set of coordi-  
 49 nates. We do not approximate the LIT using Fourier series and we do not solve any system of large dimension.  
 50 Hence, the method is not limited by memory storage (e.g. the number of Fourier coefficients needed to approxi-  
 51 mate a LIT rapidly increases with the dimension). However, in this way we do not get the parameterization of the  
 52 LIT (it has to be computed a posteriori, if required).

## 53 2 Description of the methods

54 In this section we introduce the formal approach to obtain initial conditions on a LIT using the frequency map.  
 55 Then we outline the basic ideas of the averaging-extrapolation methods that we use to compute the frequency map,  
 56 its derivatives, and the Fourier coefficients of the parameterization of the LIT. We sketch the basic formulas and  
 57 parameters of the method, and refer the reader to [25, 27, 30] for implementation details.

### 58 2.1 Setting of the problem and formal approach

59 We describe the use of the frequency map to obtain initial conditions on a LIT with prefixed frequencies. This  
 60 approach works both for Hamiltonians and symplectic maps, assuming large enough regularity. However, to  
 61 simplify the presentation, we concentrate on analytic Hamiltonians. Let  $h : U \subset \mathbb{R}^{2r} \rightarrow \mathbb{R}$  be an analytic  
 62 Hamiltonian with  $r$  degrees of freedom. We suppose  $\mathcal{T}$  is a LIT of dimension  $r$  of  $h$ , with Diophantine frequency  
 63 vector  $\omega \in \mathbb{R}^r$ :

$$|\langle k, \omega \rangle| \geq \frac{C}{|k|_1^\tau}, \quad \forall k \in \mathbb{Z}^r \setminus \{0\}, \quad |k|_1 = |k_1| + \dots + |k_r|, \quad (1)$$

64 for  $C, \tau > 0$ . This means that there is a parameterization of  $\mathcal{T}$  given by a real analytic embedding  $\varphi$  such that:

$$\varphi : \mathbb{T}^r \rightarrow \mathbb{R}^{2r}, \quad \mathcal{T} = \varphi(\mathbb{T}^r), \quad L_\omega \varphi(\theta) = J \nabla h(\varphi(\theta)), \quad (2)$$

65 where  $\mathbb{T}^r = (\mathbb{R}/2\pi\mathbb{Z})^r$ ,  $L_\omega = \sum_{j=1}^r \omega_j \partial_{\theta_j}$ , and  $J$  is the matrix of the symplectic form. We refer to (2) as the  
 66 condition of invariance of  $\varphi$ .

67 The KAM theorem ensures that, under suitable non-degeneracy conditions, there are plenty of real analytic  
 68 LITs around  $\mathcal{T}$  that are invariant by  $h$ , with frequencies moving with the torus. These LITs fill up a Cantor-like  
 69 set  $U^* \subset U$  of large Lebesgue measure. Indeed, the Lebesgue measure of the portion of the phase space not filled  
 70 up by LITs is exponentially small in the distance to  $\mathcal{T}$  (e.g. [19]). Although  $U^*$  has empty interior, these LITs  
 71 are organized as a Whitney- $\mathcal{C}^\infty$  Cantor family (e.g. [2]). Hence, there is a Cantor-like set  $\mathcal{K} \subset \mathbb{R}^r$  and functions  
 72  $\Omega : \mathcal{K} \rightarrow \mathbb{R}^r$  and  $\Psi : \mathbb{T}^r \times \mathcal{K} \rightarrow \mathbb{R}^{2r}$  such that  $\theta \mapsto \Psi(\theta, I)$  is an analytic parameterization of a LIT with  
 73 frequency vector  $\Omega(I)$ . We normalize them so that  $\varphi(\cdot) = \Psi(\cdot, 0)$  and  $\omega = \Omega(0)$ . Both,  $\Omega$  and  $\Psi$ , are Whitney- $\mathcal{C}^\infty$   
 74 functions that can be extended to  $\mathcal{C}^\infty$ -functions on open sets around  $I = 0$  and  $(\theta, I) \in \mathbb{T}^r \times \{0\}$ , respectively.  
 75 The (Kolmogorov) non-degeneracy condition at  $\mathcal{T}$  is  $\det(D\Omega(0)) \neq 0$ . We introduce the frequency map

$$\mathcal{F} : U^* \subset \mathbb{R}^{2r} \rightarrow \mathbb{R}^r \quad (3)$$

76 that assigns to any point of  $U^* = \Psi(\mathbb{T}^r \times \mathcal{K})$  the corresponding frequency vector. The value of  $\mathcal{F}(x)$  is defined  
 77 as  $\mathcal{F}(x) = \Omega(I_x)$ , with  $I_x \in \mathcal{K}$  given by the inverse of  $\Psi$ . Specifically,  $x = \Psi(\theta_x, I_x)$  for some  $\theta_x \in \mathbb{T}^r$ . Note  
 78 that the function  $\mathcal{F}(x)$  is only properly defined if  $x$  belongs to some LIT of the family. However, the Whitney- $\mathcal{C}^\infty$   
 79 character of  $\Omega$  and  $\Psi$  implies that  $\mathcal{F}$  can be extended to the whole set  $U$  as a  $\mathcal{C}^\infty$  function of the initial conditions.

80 We use the information provided by  $\mathcal{F}$  and its derivatives to compute an initial condition on  $\mathcal{T}$ . From the  
 81 practical viewpoint, we must be far away from low-order resonances. Assume that we have a point  $x^{(0)} \in U^*$ ,  
 82 close to  $\mathcal{T}$ , so that we can assign to  $x^{(0)}$  a Diophantine frequency vector  $\mathcal{F}(x^{(0)})$ . We look for a small correction  
 83  $\Delta x^{(0)} \in \mathbb{R}^{2r}$  in such a way that  $x^{(0)} + \Delta x^{(0)}$  is closer to  $\mathcal{T}$  than  $x^{(0)}$ . By the non-degeneracy of  $\mathcal{F}$ , the condition  
 84  $x^{(0)} + \Delta x^{(0)} \in \mathcal{T}$  is equivalent to the following  $r$ -dimensional nonlinear system of equations:

$$\mathcal{F}(x^{(0)} + \Delta x^{(0)}) = \omega. \quad (4)$$

85 The linearized system of (4) is given by

$$D\mathcal{F}(x^{(0)})\Delta x^{(0)} = \omega - \mathcal{F}(x^{(0)}), \quad (5)$$

86 where  $D\mathcal{F}(x^{(0)})$  is a  $r \times 2r$ -matrix of maximum range. We must add appropriate normalization conditions (de-  
 87 pending on the context at hand) to secure a single solution of (4). Our customary choice is to set to zero the value  
 88 of  $r$  coordinates of  $\Delta x^{(0)}$ . Then, we introduce the sequence  $x^{(i+1)} = x^{(i)} + \Delta x^{(i)}$  and we expect  $\mathcal{F}(x^{(i+1)})$  to take  
 89 the value  $\omega$  with an error  $\mathcal{O}(|\omega - \mathcal{F}(x^{(i)})|^2)$ . This approach can be adapted directly to several contexts: systems  
 90 depending periodically or quasi-periodically on time, iso-energetic non-degenerate conditions, exact symplectic  
 91 maps or dependence on external parameters.

92 To perform a correction of the Newton method, we follow the next basic steps:

- 93 • Let  $x^{(0)} \in U$  be a point of a LIT close to  $\mathcal{T}$ , with unknown frequency vector  $\tilde{\omega} \simeq \omega$  that verifies Diophantine  
 94 properties like (1). We introduce the sequence  $\{x_n\}$  defined by  $x_n = \phi(nT; x^{(0)})$ , where  $\phi$  is the flow of  $h$   
 95 and  $T$  is a sampling time. This sequence carries quasi-periodic motion with frequency vector  $\bar{\omega} = T\tilde{\omega}$ . To  
 96 compute  $\{x_n\}$ , and its derivatives, we have to integrate numerically the trajectory of  $x^{(0)}$  together with the  
 97 corresponding variational equations. If  $x^{(0)}$  belongs to a LIT of an exact symplectic map  $f$ , with frequency  
 98 vector  $\tilde{\omega}$ , then the sequence  $\{x_n\}$  is directly obtained as  $x_n = f^n(x^{(0)})$ , and we have  $\bar{\omega} = \tilde{\omega}$ .
- 99 • From  $\{x_n\}$  we set a complex discrete quasi-periodic signal  $\{z_n\}$  with the same frequency vector  $\bar{\omega}$ . If we  
 100 denote  $x_n = (x_n^1, \dots, x_n^r)$  we can set, for example,  $z_n = x_n^1$  or  $z_n = x_n^1 + iz_n^2$ . This choice depends on  
 101 the problem at hand. Using an averaging-extrapolation process (see Section 2.2) we construct a new quasi-  
 102 periodic signal whose rotation frequency around the origin is a selected component of  $\bar{\omega}$ . We refer to this  
 103 process as the unfolding of the signal.

- 104 • By projecting the unfolded signal we define a quasi-periodic signal of  $\mathbb{T}$ . The rotation frequency of the  
 105 projected signal is computed using averaging and extrapolation (see Section 2.3), in analogous way as it is  
 106 done in [30] for the rotation number of a map of the circle. Derivatives of the frequencies with respect to  
 107 initial conditions and parameters are computed by taking formal derivatives on the extrapolation operators.

## 108 2.2 Unfolding of the signal

109 We say that the complex sequence  $\{z_n\}_{n \in \mathbb{Z}}$  is a (discrete) quasi-periodic signal with frequency vector  $\bar{\omega} \in \mathbb{R}^r$  if  
 110 there is  $\gamma : \mathbb{T}^r \rightarrow \mathbb{C}$  such that  $z_n = \gamma(n\bar{\omega})$ ,  $\forall n \in \mathbb{Z}$ . If we denote the Fourier expansion of  $\gamma$  as

$$\gamma(\theta) = \sum_{k \in \mathbb{Z}^r} \hat{\gamma}_k e^{i\langle k, \theta \rangle}, \quad \hat{\gamma}_k = \frac{1}{(2\pi)^r} \int_{\mathbb{T}^r} \gamma(\theta) e^{-i\langle k, \theta \rangle} d\theta,$$

111 then we have the relation

$$z_n = \gamma(n\bar{\omega}) = \sum_{k \in \mathbb{Z}^r} \hat{\gamma}_k e^{in\langle k, \bar{\omega} \rangle}. \quad (6)$$

112 In this context, we say that  $\bar{\omega}$  is a Diophantine frequency vector if there exists  $\bar{C}, \tau > 0$  such that

$$|e^{i\langle k, \bar{\omega} \rangle} - 1| \geq \frac{\bar{C}}{\|k\|_1^\tau}, \quad \forall k \in \mathbb{Z}^r \setminus \{0\}. \quad (7)$$

113 The conditions in (7) for a discrete quasi-periodic signal are equivalent to say that  $(\bar{\omega}, 2\pi) \in \mathbb{R}^{r+1}$  verifies (1)  
 114 for certain  $C > 0$ . Note that the fact that  $\tilde{\omega}$  verifies (1) does not imply that  $\bar{\omega} = T\tilde{\omega}$  verifies (7). But, if  $\tilde{\omega}$  is far  
 115 away from low-order resonances, we expect  $\bar{\omega}$  to behaves like (7) for the practical viewpoint. See [27] for details.

116 Given  $\omega_0 \in \mathbb{R}$ , we introduce the recursive sums

$$\mathcal{Z}_n^{(L, \omega_0, 1)} = \sum_{m=n}^{L+n-1} z_m e^{-im\omega_0}, \quad \mathcal{Z}_n^{(L, \omega_0, p)} = \sum_{l=1}^L \mathcal{Z}_n^{(l, \omega_0, p-1)}, \quad n \geq 1, \quad L \geq 1, \quad p \geq 2, \quad (8)$$

117 and the averaged sums

$$\tilde{\mathcal{Z}}_n^{(L, \omega_0, p)} = \left[ \binom{L+p-1}{p}^{-1} \mathcal{Z}_n^{(L, \omega_0, p)} \right] e^{in\omega_0}. \quad (9)$$

118 Given the extrapolation parameters  $p_u, q_u \in \mathbb{N}$ , with  $q_u \geq p_u$ , we define the sequence

$$z_n^{(2^{q_u}, \omega_0, p_u)} = \sum_{j=0}^{p_u-1} c_j^{(p_u-1)} \tilde{\mathcal{Z}}_n^{(L_j, \omega_0, p_u)}, \quad n \geq 1, \quad (10)$$

119 where  $L_j = 2^{q_u - p_u + j + 1}$  and the (extrapolation) coefficients  $c_j^{(m)}$  are given by

$$c_j^{(m)} = (-1)^{m-j} \frac{2^{j(j+1)/2}}{\delta(j)\delta(m-j)}, \quad \delta(n) = (2^n - 1)(2^{n-1} - 1) \cdots (2^1 - 1), \quad \delta(0) = 1. \quad (11)$$

120 If  $\{z_n\}$  is an analytic signal and  $\bar{\omega}$  verifies (7), then  $\{z_n^{(2^{q_u}, \omega_0, p_u)}\}$  defines a quasi-periodic signal with frequency  
 121 vector  $\bar{\omega}$  given by the analytic function  $\gamma^{(2^{q_u}, \omega_0, p_u)} : \mathbb{T}^r \rightarrow \mathbb{C}$ . From Proposition 2.12 in [27], if  $\omega_0$  is close enough  
 122 to a particular component of  $\bar{\omega}$ , say  $\bar{\omega}_1$ , (in the sense that  $2^{q_u} |\bar{\omega}_1 - \omega_0|$  is fairly small) we have

$$|z_n^{(2^{q_u}, \omega_0, p_u)} - \hat{\gamma}_{e_1}^{(2^{q_u}, \omega_0, p_u)} e^{in\bar{\omega}_1}| = \mathcal{O}(2^{-p_u q_u}), \quad \forall n \in \mathbb{Z},$$

123 where  $\hat{\gamma}_{e_1}^{(2^{q_u}, \omega_0, p_u)}$  is the Fourier coefficient of  $\gamma^{(2^{q_u}, \omega_0, p_u)}$  associated to  $\bar{\omega}_1$ . For this reason, we say that the signal  
 124 associated to (10) gives an unfolding of order  $p_u$  of  $\{z_n\}_{n \in \mathbb{Z}}$  for the frequency  $\bar{\omega}_1$ . The construction follows using  
 125 the Richardson extrapolation method on the explicit expression of the averaged sums (9). Notice that, within the  
 126 present context, as  $\tilde{\omega} \simeq \omega$ , and the frequency vector of the target torus is known, then we can select  $\omega_0$  as  $T\omega_1$ .

127 It is worth noticing that  $\tilde{Z}_n^{(L, \omega_0, 1)}$  corresponds to the discrete Fourier transform of a sampling of  $L$  points of the  
 128 original signal, and so, there is a connection of this construction with procedures and terminology in *digital signal*  
 129 *processing* (DSP) and other methods of quasi-periodic frequency analysis (e.g. [14, 23]). In the DSP terminology,  
 130 the above construction is a linear and time-invariant *low-pass filter* that passes the frequency  $\bar{\omega}_1$  and attenuates the  
 131 remaining ones. This attenuation produces the unfolding mentioned above. We remark that this filter preserves  
 132 both the analyticity and frequency vector of the initial signal. If high-frequency oscillations are sufficiently atten-  
 133 uated, then  $\bar{\omega}_1$  becomes the rotation frequency around the origin (i.e.  $\bar{\omega}_1/2\pi$  is the average number of turns of the  
 134 unfolded signal around the origin).

135 The fact that  $\bar{\omega}_1$  is the rotation frequency means that if we consider the projection to  $\mathbb{T}$

$$x_n^{(2^{q_u}, \omega_1^0, p_u)} = \arg(z_n^{(2^{q_u}, \omega_1^0, p_u)}), \quad (12)$$

136 then we can write

$$x_n^{(2^{q_u}, \omega_1^0, p_u)} = n\bar{\omega}_1 + X^{(2^{q_u}, \omega_1^0, p_u)}(n\bar{\omega}), \quad (13)$$

137 where  $X^{(2^{q_u}, \omega_1^0, p_u)} : \mathbb{T}^r \rightarrow \mathbb{R}$  is an analytic function. The expression (13) denotes the lift to  $\mathbb{R}$  of the projected  
 138 signal rather than the signal of  $\mathbb{T}$  itself (i.e. the argument must be increased by  $2\pi$  whenever  $z_n^{(L, \omega_1^0, p_u)}$  completes  
 139 one turn around the origin). In practice, we say that the unfolding of the signal  $\{z_n\}$  has succeeded if we can  
 140 set  $\bar{\omega}_1$  as the value of the rotation frequency and if we are able to track the evolution of the argument along the  
 141 unfolded iterates. Notice that we do not need  $X^{(2^{q_u}, \omega_1^0, p_u)}$  to be small, and its effect will be averaged out when  
 142 computing the rotation frequency in Section 2.3. Consequently, taking values  $p_u = 2$  and  $q_u = 10$  is enough in  
 143 most situations. We refer to [27] for efficient recurrences to compute the unfolded signal.

144 Although we have described the unfolding process corresponding to a particular frequency  $\bar{\omega}_1$ , in practice we  
 145 perform this process simultaneously for all the components of  $\bar{\omega}$ . In this way, we do not need to store in memory  
 146 the integration sample and we also save several loops in the algorithm.

### 147 2.3 Computation of the frequency vector and derivatives

148 We introduce the recursive sums

$$S_n^{(0)} = x_n^{(2^{q_u}, \omega_1^0, p_u)}, \quad S_n^{(p)} = \sum_{m=1}^n S_m^{(p-1)}, \quad n \geq 1, \quad p \geq 1. \quad (14)$$

149 Given  $p_r, q_r \in \mathbb{N}$ , with  $q_r \geq p_r$ , we introduce the operator

$$\Theta^{(p_r, q_r)} = \sum_{j=0}^{p_r} c_j^{(p_r)} \binom{N_j + p_r}{p_r + 1}^{-1} S_{N_j}^{(p_r)}, \quad (15)$$

150 where  $N_j = 2^{q_r - p_r + j}$ , and the coefficients  $c_j^{(m)}$  are given by (11). If equation (13) holds, it turns out that

$$\bar{\omega}_1 = \Theta^{(p_r, q_r)} + \mathcal{O}(2^{-q_r(p_r+1)}).$$

151 We refer the reader to [27, 30] for justifications, details on optimal selection of the parameters  $p_r$  and  $q_r$ , and  
 152 complete description of implementation details. We observe that to compute the recursive sums  $\{S_{N_j}^{(p_r)}\}_{j=0}^{p_r}$  we

153 only need to store in memory a  $(p_r + 1) \times (p_r + 1)$  matrix array. We do not need to store the iterates of the signal.  
 154 We also point out the recent work [6] for a similar approach to the computation of rotation frequencies.

155 Assume that the problem depends (at least  $\mathcal{C}^1$ ) on a parameter  $\alpha$ . We observe that the linear structure of the  
 156 operator  $\Theta^{(p_r, q_r)}$  (and of the unfolding procedure of Section 2.2) commutes with the differential operator  $\partial_\alpha$ . For  
 157 this reason, the above method can be directly extended to compute derivatives with respect to parameters. Hence,  
 158 we can compute approximations of  $\partial_\alpha \bar{\omega}_1$  by taking formal derivatives on these operators. Then, we introduce the  
 159 sums  $\partial_\alpha S_{N_j}^{(p_r)}$ , associated to  $\{\partial_\alpha x_n^{(L, \omega_1^0, p_u)}\}$ , using the same recurrences as in (14), and we obtain

$$\partial_\alpha \bar{\omega}_1 = \partial_\alpha \Theta^{(p_r, q_r)} + \mathcal{O}(2^{-q_r p_r}).$$

160 We refer the reader to [24, 25] for an exhaustive discussion and implementation details. If the signal is given  
 161 through a Hamiltonian flow or a symplectic map, we cannot expect it to be well-defined for every value  $\alpha$ , but only  
 162 for a Cantor set. According to the discussions in Section 2.1, we expect that  $\partial_\alpha \bar{\omega}(\alpha)$  is well defined in the sense  
 163 of Whitney. We remark that the method works for computing higher order derivatives of  $\bar{\omega}_1$ , but the computations  
 164 become more difficult when the order increases. Specifically, for a derivative of order  $d$  the extrapolation error is  
 165 controlled by  $\mathcal{O}(2^{-q_r(p_r+1-d)})$ .

166 To perform our methodology we have to compute a sample of  $M$  points of this signal, as well as its derivatives  
 167 with respect to initial conditions and parameters. Note that if we unfold the signal using parameter values  $p_u$  and  
 168  $q_u$  and we refine the frequencies using parameter values  $p_r$  and  $q_r$ , then  $M = 2^{q_u} + 2^{q_r} - 1$ .

## 169 2.4 Computation of the Fourier coefficients

170 In many applications, we may be interested in computing the parameterization  $\varphi$  of a LIT rather than a single point  
 171 on it. By computing several Fourier coefficients of  $\varphi$  we obtain an initial guess to use the parameterization method  
 172 in KAM theory (e.g. [8, 15, 18]). It turns out that the averaging-extrapolation method can be adapted to deal with  
 173 this scenario.

174 Let  $\mathcal{T}$  be a LIT with frequency vector  $\omega$  and assume that we have computed  $x^* \in \mathcal{T}$  by solving (4). Let  
 175  $\varphi : \mathbb{T}^r \rightarrow \mathbb{R}^{2r}$  be the parameterization of  $\mathcal{T}$ , given by (2), such that  $\varphi(0) = x^*$  and let  $\{\hat{\varphi}_k\}_{k \in \mathbb{Z}^r}$  be the Fourier co-  
 176 efficients of  $\varphi$ . Unfortunately, we cannot obtain  $\{\hat{\varphi}_k\}_{k \in \mathbb{Z}^r}$  directly by DFT since we only can evaluate a trajectory  
 177 on the LIT, and so, we cannot generate the values of  $\varphi$  on an equispaced grid of points on  $\mathbb{T}^r$ . As this trajectory  
 178 is dense on  $\mathcal{T}$ , we have the option of using interpolation to get approximations to the values of  $\varphi$  on the grid, but  
 179 the error of interpolation can be large when  $r$  increases. Next, we explain how we can get Fourier coefficients by  
 180 averaging an extrapolation.

181 We consider the signal  $\{x_n\}$ , with  $x_n = \phi(nT; x^*)$ , where  $\phi$  is the flow of  $h$  and  $T$  is the sampling time. Then,  
 182 the frequency vector of this signal is  $T\omega$ . The computed values satisfy  $x_n = \varphi(nT\omega)$ . Hence, the corresponding  
 183 points of  $\mathbb{T}^r$  are not equispaced, but distributed according to the translational dynamics by  $T\omega$ . Given a fixed  
 184  $k \in \mathbb{Z}^r$ , the expression  $x_n^{(k)} = x_n e^{-inT\langle k, \omega \rangle}$  defines a discrete quasi-periodic signal of  $\mathbb{C}^{2r}$  with frequency vector  
 185  $T\omega$  and average  $\hat{\varphi}_k$ . We introduce the recursive sums

$$S_n^{(0)}(k) = x_n^{(k)}, \quad S_n^{(p)}(k) = \sum_{m=1}^n S_m^{(p-1)}(k), \quad n \geq 1 \quad p \geq 1. \quad (16)$$

186 Given  $p_f, q_f \in \mathbb{N}$ , with  $q_f \geq p_f$ , we introduce the operator

$$\Gamma_k^{(q_f, p_f)} = \sum_{j=0}^{p_f-1} c_j^{(p_f-1)} \binom{N_j + p_f - 1}{p_f}^{-1} S_{N_j}^{(p_f)}(k), \quad (17)$$

187 where  $N_j = 2^{q_f - p_f + j + 1}$  and the coefficients  $c_j^{(p_f - 1)}$  are given by (11). Then, it turns out that

$$\hat{\gamma}_k = \Gamma_k^{(p_f, q_f)} + \mathcal{O}(2^{-q_f p_f}).$$

188 We refer the reader to [27] for a complete description of implementation details.

189 In practice, it may be interesting to take  $p_f = p_r + 1$  and  $q_f = q_r$ . Then the operators in (15) and (17)  
 190 are applied to the same sample of  $N = 2^{q_r}$  iterates. Using the operator (17), we can compute a selected set of  
 191 Fourier coefficients, with high precision, independently of the other ones. Among the drawbacks of this approach,  
 192 we stress the fact that we miss the orthogonality properties of the DFT. This lack of orthogonality increases the  
 193 perturbative effect of the dominant Fourier coefficients when computing  $\hat{\varphi}_k$  for large values of  $|k|$ . For this reason,  
 194 it may be a good idea to start by computing the dominant part of  $\varphi$ . If we subtract this from the signal, then we  
 195 magnify the contribution of the high order frequencies (this is a typical approach when performing a quasi-periodic  
 196 frequency analysis with methods based on DFT, e.g. [14, 23]). We remark again that an interesting possibility is to  
 197 compute a rough approximation to  $\varphi$ , and then to refine it by means of a parameterization method. An analogous  
 198 strategy is useful if we want a point on  $\mathcal{T}$ , but “far away” from  $x^*$  (e.g., the intersection of  $\mathcal{T}$  with a certain  
 199 transverse manifold). We can use a rough approximation to  $\varphi$  to locate a point close to  $\mathcal{T}$  verifying also the desired  
 200 properties. Then, we can refine this point by the methodology of this paper.

201 Finally, we can use the extrapolation operator (17) to validate the computation of the frequency in Section 2.3.  
 202 Assume that we want to check whether  $\Theta^{(p_r, q_r)}$  provides a true approximation to  $\bar{\omega}_1$ . We can proceed by computing  
 203 the Fourier coefficient  $\hat{\gamma}_{e_1}$  associated to this frequency, using  $\Theta^{(p_r, q_r)}$  to compute  $x_n^{(e_1)}$ . If  $\Theta^{(p_r, q_r)}$  approximates  
 204 a frequency of  $\{z_n\}$ , then  $\hat{\gamma}_{e_1} \neq 0$ . Accordingly, if we numerically obtain that  $\hat{\gamma}_{e_1} = 0$ , then  $\Theta^{(p_r, q_r)}$  is not an  
 205 approximation to  $\bar{\omega}_1$ . In this case we must improve the unfolding process by taking a larger value of  $L$  to define  
 206 each unfolded iterate or by looking for a better approximation to  $\bar{\omega}_1$  than  $\omega_1^0$ .

### 207 3 Numerical examples

208 We consider two different examples in order to enhance the main features and limitations of the presented meth-  
 209 ods. In Section 3.1 we study a simple model that describes a coupled chain of anharmonic oscillators. The main  
 210 reason for considering this discrete-time system is because dealing with this symplectic map we can easily compute  
 211 a large number of iterates with a simple implementation and fast computational time. In Section 3.2 we compute  
 212 some families of LITs in a Restricted Three Body Problem. We consider different situations involving the planar  
 213 and the spatial cases, and also the circular and the elliptic cases.

#### 214 3.1 A model of coupled anharmonic oscillators

215  
 216 The considered FPU model is a discretization of a canonical model describing  $r$  anharmonic oscillators with a  
 217 local coupling that has been extensively studied in the literature (e.g. [1, 16]) after the pioneering work of Fermi,  
 218 Pasta and Ulam in [10]. We consider  $x \in \mathbb{T}^r$  and  $y \in \mathbb{R}^r$ , where we set  $\mathbb{T} = \mathbb{R}/\mathbb{Z}$  in order to follow the common  
 219 convention in the literature. Then, the dynamics is given by the exact symplectic map  $(\bar{x}, \bar{y}) = F(x, y)$  defined as

$$\bar{x}_i = x_i + \bar{y}_i, \quad \bar{y}_i = y_i - \frac{\alpha_i}{2\pi} \sin(2\pi x_i) + \frac{\beta}{2\pi} \sin(2\pi(x_{i+1} - x_i)) - \frac{\beta}{2\pi} \sin(2\pi(x_i - x_{i-1})), \quad (18)$$

220 for  $i = 1, \dots, r$ , where we identify  $x_0 = x_r$  and  $x_{r+1} = x_1$ . The parameters  $\{\alpha_i\}_{i=1}^r$  are associated to the  
 221 anharmonic oscillators and  $\beta$  measures the coupling between the oscillators. Notice that each iterate is obtained  
 222 just by evaluating  $2r$  times the sinus function and performing few elemental operations. Hence, we can compute

223 a huge number of iterates of the map (18), as well as its derivatives, up to a high accuracy but with a moderate  
 224 computational cost. To exploit this fact, we perform computations using an arithmetic of 32 decimal digits.

225 In this example, we use  $p_u = 2$  and  $q_u = 10$  for the unfolding procedure and we use  $p_r = 8$  and  $q_r \leq 20$  for  
 226 the computation of the frequencies and its derivatives. We compute approximations to the frequencies using  $2^{q_r}$   
 227 unfolded iterates, increasing the value of  $q_r$  from 8 to 20. We stop when the difference between two consecutive  
 228 approximations is smaller than a prefixed tolerance. Approximations of the derivatives of the frequencies are com-  
 229 puted by using the same number of iterates needed to validate the frequencies. The tolerance for the computation  
 230 of the frequencies and the tolerance for the Newton method are selected according to each particular situation.

231 For  $\beta = 0$  the model (18) turns out to be the product of  $r$  uncoupled standard maps [5] of the form

$$(x, y) \mapsto \left( \bar{x} = x + \bar{y}, \bar{y} = y - \frac{\alpha}{2\pi} \sin(2\pi x) \right). \quad (19)$$

232 For  $\alpha = 0$ , the circles  $\mathbb{T} \times \{\omega\}$  are invariant and with rotation number  $\omega$ . If  $\omega$  is Diophantine and  $|\alpha|$  is small  
 233 enough, the map (19) has an invariant curve with rotation number  $\omega$ . Since (19) is a twist map, the projection of  
 234 this invariant curve onto  $\mathbb{T}$  defines a circle map with rotation number  $\omega$ . This fact allows performing the numerical  
 235 continuation with respect to  $\alpha$  of an initial condition on this curve, without needing to carry out the unfolding  
 236 procedure. Hence, we obtain an analytic curve  $y^0(\alpha)$  so that  $(0, y^0(\alpha))$  belongs to an invariant curve of (19) with  
 237 rotation number  $\omega$ . We refer the reader to [25, 30] for details on this specific continuation. This curve is used later  
 238 on to initialize the computation of LITs of (18) for higher number of coupled oscillators.

239 For  $r = 2$  the model (18) defines a Froeschlé-like map  $F_{\alpha_1, \alpha_2, \beta}$ . The Froeschlé map [11] has been used as a  
 240 model to understand instability channels. In this case, we can only ensure that the direct projection of the iterates  
 241 onto the angular variables  $(x_1, x_2) \in \mathbb{T}^2$  is well-posed if  $|\alpha|, |\beta| \ll 1$ . For general values of  $\alpha$  and  $\beta$ , we should  
 242 use the unfolding procedure. We fix a Diophantine rotation vector  $\omega^0 = (\omega_1^0, \omega_2^0)$  (i.e., the frequency vector is  
 243  $2\pi\omega^0$ ) and we consider the LIT of  $F_{\alpha_1, \alpha_2, \beta}$ , for  $\beta = 0$ , defined as the product of the invariant curves of (19) for  
 244  $\alpha = \alpha_1$  and  $\alpha = \alpha_2$ , with rotation number  $\omega_1^0$  and  $\omega_2^0$ , respectively. Then, we fix the values  $\alpha_1$  and  $\alpha_2$ , and we  
 245 perform the numerical continuation with respect to  $\beta$  of the LIT of  $F_{\alpha_1, \alpha_2, \beta}$  with rotation frequency  $\omega^0$ . To apply  
 246 the methods of Section 2, we consider initial conditions of the form  $(x_1^0, x_2^0, y_1^0, y_2^0)$ , with  $x_1^0 = 0$ , and  $x_2^0 = 0$ , and  
 247 we deal with the complex signal

$$z_n = (1 + y_1^n) e^{2\pi i x_1^n} + (1 + y_2^n) e^{2\pi i x_2^n},$$

248 that is defined in terms of the orbit  $(x_1^n, x_2^n, y_1^n, y_2^n) = F_{\alpha_1, \alpha_2, \beta}^n(0, 0, y_1^0, y_2^0)$ . Abusing notation, we denote by  $\omega_1$   
 249 and  $\omega_2$  the components of the frequency map of  $F_{\alpha_1, \alpha_2, \beta}$ . Since the values of  $\alpha_1$  and  $\alpha_2$  are fixed, and we select  
 250 initial conditions with  $x_1^0 = 0$  and  $x_2^0 = 0$ , we have to evaluate the derivatives

$$\frac{\partial \omega_1}{\partial y_1^0}, \quad \frac{\partial \omega_1}{\partial y_2^0}, \quad \frac{\partial \omega_1}{\partial \beta}, \quad \frac{\partial \omega_2}{\partial y_1^0}, \quad \frac{\partial \omega_2}{\partial y_2^0}, \quad \frac{\partial \omega_2}{\partial \beta}. \quad (20)$$

251 As a specific example, we consider the rotation vector  $\omega^0 = (\sqrt{2} - 1, \sqrt{3} - 1)$ , and we fix  $\alpha_1 = 0.1$  and  
 252  $\alpha_2 = 0.2$ . We ask for a tolerance of  $10^{-23}$  in the computation of frequencies. If the error of the frequencies is larger  
 253 than  $10^{-20}$  after we reach the value  $q_r = 20$ , then we do not validate the results and we stop the computations. To  
 254 perform the Newton method on the frequency map, we ask for a tolerance of  $10^{-20}$  (i.e., we validate the results  
 255 when the frequency map equals to  $\omega^0$  up to this tolerance). Results of this continuation are shown in the red curve  
 256 of Fig. 1. The computation performs with significant accuracy (around 23 decimal digits for frequencies and 19  
 257 decimal digits for derivatives) up to  $\beta \simeq 0.015$ . Beyond this point, as we approach to the breakdown of the LIT,  
 258 the width of the strip of analyticity of the parameterization shrinks. This loss of regularity affects the precision of  
 259 the averaging-extrapolation methods. Anyway, we are still able to compute an initial condition on the LIT with  
 260 at least 20 decimal digits up to the value  $\beta \simeq 0.02778$ . Although for larger values of  $\beta$  we cannot keep such



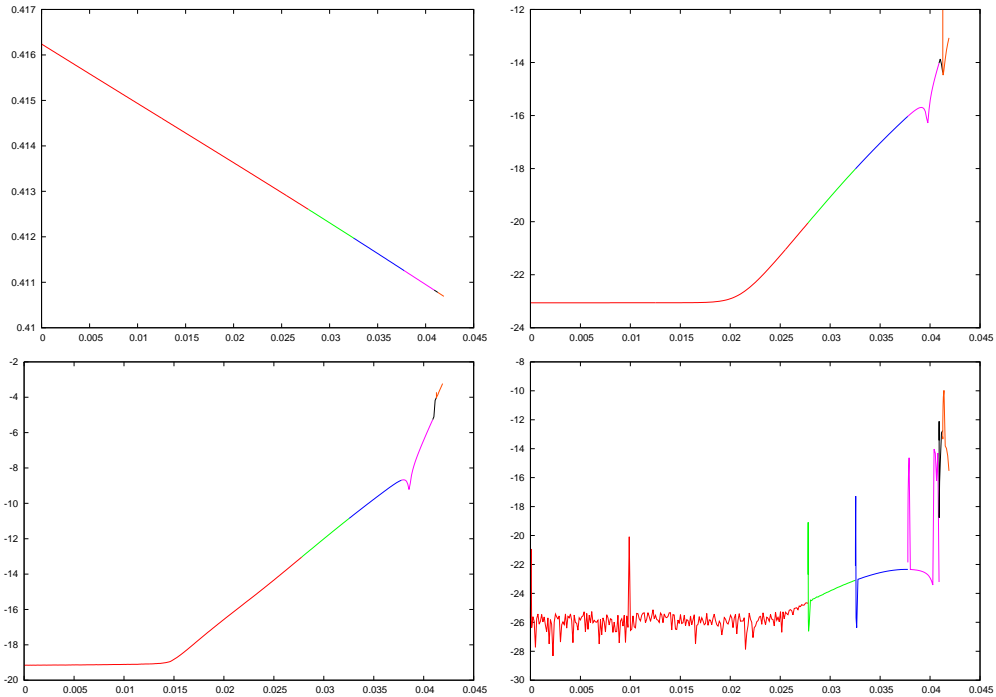


Figure 1: Numerical continuation w.r.t.  $\beta$  (horizontal axis) of the LIT of rotation vector  $(\omega_1^0, \omega_2^0) = (\sqrt{2} - 1, \sqrt{3} - 1)$  of (18) for  $\alpha_1 = 0.1$ , and  $\alpha_2 = 0.2$ . Colors correspond to the tolerance in the Newton method (see Table 1). Top-Left: initial condition  $y_1^0$ . Top-Right:  $\log_{10}$  of the averaged extrapolation error in the computation of the two frequencies. Bottom-Left:  $\log_{10}$  of the averaged extrapolation error in the computation of the six derivatives in (20). Bottom-Right:  $\log_{10}$  of the error in the convergence of the Newton method.

Color	Tol. freq.	Tol. New.	Last computed $\beta$
Red	$10^{-23}$	$10^{-20}$	0.0277810751329753802587
Green	$10^{-21}$	$10^{-18}$	0.0325299413989953885507
Blue	$10^{-18}$	$10^{-16}$	0.0377754515433391344838
Magenta	$10^{-16}$	$10^{-14}$	0.0408963352103296900526
Black	$10^{-14}$	$10^{-12}$	0.0412699621910886738677
Orange	$10^{-12}$	$10^{-10}$	0.0418933219731313588506

Table 1: Implementation parameters of the Newton method corresponding to the colored curves shown in Figs. 1 and 2. The rightmost column is the value of the parameter  $\beta$  for the last computed LIT in the curve.

261 level of accuracy, we still observe a nice and regular performance of the extrapolation methods in general and,  
 262 particularly, in the computation of the derivatives. Accordingly, we expect the LIT to exist beyond the red curve.  
 263 To carry out the continuation for  $\beta > 0.02778$ , we ask for a higher tolerance in the Newton method. Results of the  
 264 continuation under less demanding tolerances are shown, using different colors, in Figs. 1 and 2. The information  
 265 corresponding to the color scale is given in Table 1. We note that the accuracy of the derivatives (20) decreases as  $\beta$   
 266 approach to the last computed value  $\beta \simeq 0.04189$ . The asymptotic behavior of the size of these derivatives shows  
 267 that this value is close to the blow up of the derivatives with respect to parameters. Hence, we are approaching to  
 268 the breakdown of the LIT.

269 In order to illustrate the performance of the method when the dimension of the LIT (i.e., the number of fre-  
 270 quencies) increases, we continue with respect to  $\beta$  a LIT of (18) for  $r = 4$  and  $r = 8$ . Results for  $r = 4$  are  
 271 displayed in Table 3 and correspond to  $\alpha_1 = 0.1$ ,  $\alpha_2 = 0.2$ ,  $\alpha_3 = 0.1$ ,  $\alpha_4 = 0.2$ , and rotation frequencies

$$\omega^0 = (\sqrt{2} - 1, \sqrt{3} - 1, \sqrt{5} - 2, \sqrt{7} - 2), \quad (21)$$

$\beta$	$y_1^0$	$y_2^0$	$ \omega_1 - \omega_1^0 $	$ \omega_2 - \omega_2^0 $
9.77716914081557254627e-07	0.416239280635578818468	0.717977454920173053136	1e-26	2e-26
5.38089767561550300719e-03	0.415535218621395843133	0.718890011733364250169	2e-26	1e-25
1.10137539367116352242e-02	0.414801405234141105449	0.719843976010496173569	2e-27	2e-26
1.68967198315117365065e-02	0.414035543304713472584	0.720842185525490944118	2e-27	4e-26
2.24027813672504887457e-02	0.413315391788239314504	0.721782443104299664683	2e-26	1e-26
2.77810751329753802587e-02	0.412604505093834489587	0.722711201685412677265	1e-24	2e-24
2.94053945778807538302e-02	0.412387760166496501515	0.722994356653690987061	6e-24	8e-24
3.15302331705021581937e-02	0.412102611401104060735	0.723366816598592656407	3e-23	3e-23
3.34036002738324504311e-02	0.411849701084173189480	0.723697108382632535398	9e-23	1e-22
3.65265450798611782387e-02	0.411425308486084343014	0.724251278520835355351	2e-22	3e-22
3.80242428972714170416e-02	0.411220816608226213801	0.724518316461670266277	2e-22	3e-22
3.93978946891543367520e-02	0.411032905535375449688	0.724763742955280848283	1e-22	2e-22
4.08963352103296900526e-02	0.410827708715062350638	0.725031821789886603282	3e-23	5e-23

Table 2: Some output data of the numerical continuation with respect to  $\beta$  of Figs. 1 and 2. In the last two columns we show the estimated error obtained for the frequencies in the Newton method.

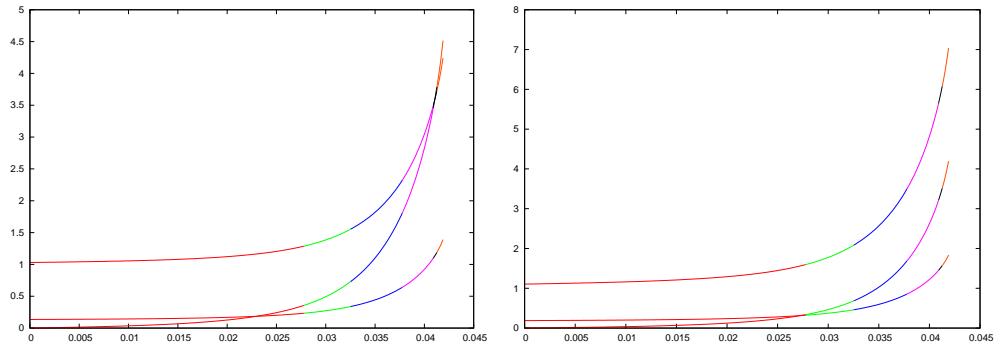


Figure 2: Additional plots to the numerical continuation with respect to  $\beta$  of Fig. 1. Left: Absolute value of the derivatives of  $\omega_1$  with respect to  $(y_1^0, y_2^0, \beta)$ . Right: Absolute value of the derivatives of  $\omega_2$  with respect to  $(y_1^0, y_2^0, \beta)$ .

$\beta$	$y_1^0$	$y_2^0$	$y_3^0$	$y_4^0$	$ \omega - \omega^0 $
9.779439684885e-07	0.4162392678913	0.7179773739847	0.2447614664937	0.6381604610137	1e-25
1.242005127722e-04	0.4162214880000	0.7179880933506	0.2447554403886	0.6381754561794	4e-27
4.997557667751e-04	0.4161672921146	0.7180206035566	0.2447372441062	0.6382211619743	9e-27
6.317939443707e-04	0.4161482354020	0.7180319763522	0.2447309074316	0.6382372326375	3e-23
9.995637966472e-04	0.4160951491976	0.7180634968389	0.2447134243981	0.6382819984438	3e-17
1.625618649899e-03	0.4160047558418	0.7181166259178	0.2446842270968	0.6383582157448	5e-17
2.251751970294e-03	0.4159143181082	0.7181690986610	0.2446557367438	0.6384344580512	5e-17
2.751735327176e-03	0.4158420760031	0.7182105254825	0.2446334967205	0.6384953503886	3e-17
3.503267593603e-03	0.4157334427959	0.7182720067843	0.2446009199017	0.6385868964559	1e-16
4.254904463352e-03	0.4156247366839	0.7183325551101	0.2445693631055	0.6386784763119	9e-16
4.881346034123e-03	0.4155340898778	0.7183823029776	0.2445438461321	0.6387548179573	2e-15
5.383527613237e-03	0.4154613909064	0.7184217156897	0.2445239058184	0.6388160265805	1e-14
5.397232974486e-03	0.4154594064151	0.7184227855827	0.2445233679744	0.6388176971853	1e-12

Table 3: Some output data of the numerical continuation with respect to  $\beta$  of the LIT of (18) of rotation frequencies (21) for  $\alpha_1 = \alpha_3 = 0.1$  and  $\alpha_2 = \alpha_4 = 0.2$ . In the last column we show the sum of the estimated error obtained for the frequencies after the Newton method.

272 Results for  $r = 8$  are displayed in Table 4 and correspond to  $\alpha_i = 0.1, i = 1, \dots, 8$ , and

$$\omega^0 = (\sqrt{2} - 1, \sqrt{3} - 1, \sqrt{5} - 2, \sqrt{7} - 2, \sqrt{11} - 3, \sqrt{13} - 3, \sqrt{17} - 4, \sqrt{19} - 4). \quad (22)$$

273 If we focus on the last columns of Tables 3 and 4, we observe how the accuracy of the results is reduced as we  
274 approach to the breakdown of the LIT.

$\beta$	$y_1^0$ & $y_5^0$	$y_2^0$ & $y_6^0$	$y_3^0$ & $y_7^0$	$y_4^0$ & $y_8^0$	$ \omega - \omega^0 $
8.721026636145e-07	0.4162397440728 0.3217096059857	0.7249722133046 0.6029467432330	0.2447614773163 0.1431926686372	0.6419081663358 0.3625911181005	2e-23
6.104690229538e-06	0.4162417545974 0.3217089437365	0.7249725942790 0.6029470295899	0.2447612546689 0.1431922227900	0.6419086441563 0.3625892646069	5e-21
2.703455495136e-05	0.4162497977287 0.3217062949516	0.7249741172879 0.6029481748676	0.2447603646304 0.1431904395238	0.6419105550262 0.3625818498993	1e-18
1.107463501067e-04	0.4162819867430 0.3216957036192	0.7249801951158 0.6029527535822	0.2447568132825 0.1431833083655	0.6419181915871 0.3625521793992	3e-16
3.339203121380e-04	0.4163679521865 0.3216674995059	0.7249962918378 0.6029649448522	0.2447474116802 0.1431643056256	0.6419384941006 0.3624729682366	5e-15
5.570164172625e-04	0.4164541018311 0.3216393752779	0.7250122280960 0.6029771092797	0.2447381094064 0.1431453199186	0.6419586893359 0.3623936297754	4e-15
7.800418216508e-04	0.4165404330789 0.3216113592776	0.7250280047780 0.6029892471999	0.2447289057641 0.1431263476848	0.6419787550248 0.3623141682097	8e-15

Table 4: Some output data of the numerical continuation with respect to  $\beta$  of the LIT of (18) of rotation frequencies (22) for  $\alpha_i = 0.1$ ,  $i = 1, \dots, 8$ . In the last column we show the sum of the estimated error obtained for the frequencies after the Newton method.

### 3.2 Study of a Restricted Three Body Problem

We consider two punctual masses (called primaries) describing an elliptic orbit, according to the Newton laws, with eccentricity  $e$  and semimajor axis  $a$ . The elliptic restricted three body problem (ERTBP) describes the motion of a third massless particle (an asteroid) under the gravitational attraction of the primaries. As usual, we consider a rotating coordinate system with origin at the center of mass of the primaries, so that the two primaries are fixed on the  $x$ -axis, the  $z$ -axis has the direction of the angular momentum and the  $y$ -axis is defined to have a positive-oriented frame. If we choose units of distance, time, and mass such that  $a = 1$ , the period is  $2\pi$  and the sum of the masses is 1, and we take as independent variable the true anomaly  $f$ , then the Hamiltonian  $H_e = H_e(x, y, z, p_x, p_y, p_z, f)$  for the third particle is  $2\pi$ -periodic on  $f$  and is given by (e.g. [32])

$$H_e = \frac{(p_x + y)^2 + (p_y - x)^2 + p_z^2 + z^2}{2} - \frac{1}{E} \left[ \frac{x^2 + y^2 + z^2}{2} + \frac{1 - \mu}{r_1} + \frac{\mu}{r_2} \right], \quad (23)$$

where  $E = 1 + e \cos f$ ,  $p_x = \dot{x} - y$ ,  $p_y = \dot{y} + x$ ,  $p_z = \dot{z}$ ,  $r_1^2 = (x - \mu)^2 + y^2 + z^2$ ,  $r_2^2 = (x - \mu + 1)^2 + y^2 + z^2$ , and  $\mu \in (0, \frac{1}{2}]$  is the mass of the smallest primary. The connection between  $f$  and the time  $t$  is given by:

$$\dot{f} = (1 - e^2)^{-3/2} (1 + e \cos f)^2. \quad (24)$$

For  $e = 0$ , we obtain the Circular Restricted Three Body Problem (CRTBP), given by the autonomous Hamiltonian

$$H_0(x, y, z, p_x, p_y, p_z) = \frac{p_x^2 + p_y^2 + p_z^2}{2} + yp_x - xp_y - \frac{1 - \mu}{r_1} - \frac{\mu}{r_2}. \quad (25)$$

Although for  $e \neq 0$  the Hamiltonian (23) is  $2\pi$ -periodic, it has five equilibrium points. Three of them (the Eulerian points  $L_1$ ,  $L_2$ , and  $L_3$ ) are on the  $x$  axis, and the other two (the Lagrangian points  $L_4$  and  $L_5$ ) are on the plane  $xy$  and form an equilateral triangle with the primaries. We focus on  $L_5$  (the point  $L_4$  is equivalent), given by  $(\mu - \frac{1}{2}, \frac{\sqrt{3}}{2}, 0, -\frac{\sqrt{3}}{2}, -\frac{1}{2} + \mu, 0)$ . It is well-known that for  $e = 0$  and  $0 < \mu < \mu_R$ , where  $\mu_R = \frac{1}{2}(1 - \sqrt{23/27}) \simeq 0.03852$  is the Routh critical value, the point  $L_5$  is linearly stable (elliptic) with normal frequencies

$$\omega_1^{(L_5)} = \left[ \frac{1}{2} (1 - (1 - 27\mu(1 - \mu))^{1/2}) \right]^{1/2}, \quad \omega_2^{(L_5)} = \left[ \frac{1}{2} (1 + (1 - 27\mu(1 - \mu))^{1/2}) \right]^{1/2}, \quad (26)$$

and  $\omega_3^{(L_5)} = 1$  (the one of the vertical oscillations).

294 In this section we use the Newton method on the frequency map to compute and continue numerically LITs  
 295 around  $L_5$  of the CRTBP and the ERTBP for the Sun-Jupiter system, given by  $\mu_{SJ} = 0.00095388118$ . KAM  
 296 theory (e.g. [19, 20]) predicts that there is a large set of LITs around  $L_5$ . For  $e = 0$ , the frequency analysis of the  
 297 CRTBP for  $\mu = \mu_{SJ}$  shows that  $L_5$  is stable from the effective viewpoint (e.g. [14, 27]) in a domain larger than  
 298 the one for which the existence of LITs has been established (e.g. [4, 14]).

299 In the computations performed bellow we consider initial conditions close to  $L_5$  parameterized as follows:

$$x = \mu + (1 + \rho) \cos(2\pi x), \quad y = (1 + \rho) \sin(2\pi x), \quad z = z, \quad \dot{x} = \dot{y} = \dot{z} = 0, \quad f = 0.$$

300 This selection of variables  $(\alpha, \rho)$  is suitably adapted to the shape of the domain of stability of the problem. Taking  
 301 zero velocity is a normalization condition for the LIT. Given an initial condition of this form, we assume that the  
 302 corresponding trajectory belongs to a LIT of the system (with three frequencies for the CRTBP and four frequencies  
 303 for the ERTBP). For  $e \neq 0$  the time-frequency is known, so we focus on the remaining ones. For small values  
 304 of  $e$ , these frequencies are close to the ones of  $L_5$  for the CRTBP (see (26)). In particular, the motion restricted  
 305 to the plane  $z = 0$  has only two frequencies. We address the computation of the frequency map in terms of the  
 306 complex signal  $x_n + iy_n - \Gamma$ , where the values of  $x_n$  and  $y_n$  are defined by using sampling time  $T = 1$ . This  
 307 implies that the frequencies of the discrete signal are the same as those of the continuous one. The value of  $\Gamma$  is  
 308 an approximation to the average of the discrete signal, computed using with  $p_f = 2$  and  $q_f = 10$ . Notice that  
 309 removing the average of the signal is a useful trick to accelerate the convergence of the unfolding process. We use  
 310 the extrapolation parameters  $p_u = 2$  and  $q_u = 10$  for the unfolding procedure and we use  $p_r = 5$  and  $q_r \leq 16$  for  
 311 the computation of the frequencies and its derivatives. To integrate the Hamiltonian  $H_e$  we use a Taylor method of  
 312 order 22 and double precision arithmetic.

### 313 3.2.1 The planar case

314 To illustrate the flexibility of our approach, we perform different continuations of LITs of the planar CRTBP  
 315 following several criteria. As starting point, we consider the initial condition given by

$$\alpha = 0.28, \quad \rho = 0, \quad z = 0. \quad (27)$$

316 By performing frequency analysis of the corresponding trajectory (e.g. [27]) we obtain the frequencies

$$\omega_1^0/2\pi = 0.01258702486754, \quad \omega_2^0/2\pi = 0.15861068715732. \quad (28)$$

317 To perform the computations, we ask for a tolerance of  $10^{-14}$  in the computation of frequencies (but we do not  
 318 explicitly control the accuracy of its derivatives) and a tolerance of  $10^{-10}$  for the Newton method.

319 First, we continue LITs by fixing the value of one of the frequencies. Abusing notation, we denote by  $(\omega_1, \omega_2)$   
 320 the components of the frequency map as function of the initial values  $\rho^0$  and  $\alpha^0$ . Then, the considered equations  
 321 are  $\omega_1 = \omega_1^0$  and  $\omega_2 = \omega_2^0$ . Each of these equations defines a curve on the plane  $\alpha^0 \rho^0$ . Note that there is a dense  
 322 set of resonances as the other frequency moves along the curve. However, due to the large density of LITs we  
 323 do not observe these holes numerically. Both curves are shown in the left plot of Fig. 3 and they define a convex  
 324 domain around the point  $(\alpha^0, \rho^0) = (1/3, 0)$ , that corresponds to  $L_5$ . These curves are very close to each other.  
 325 In the right plot in Fig. 3 we display a zoom to show that they are different. This close-to-degenerate behavior is  
 326 typically observed in celestial mechanics, since it is common that frequencies move very slowly with respect to  
 327 initial conditions.

328 Next, we deal with the iso-energetic continuation  $\omega_2/\omega_1 = \omega_2^0/\omega_1^0$  using the energy  $E = H_0$  as a parameter.  
 329 Now, we obtain a continuous curve very similar to the left plot of Fig. 3. In the same way, the value of  $\lambda$  defined by  
 330  $(\omega_1, \omega_2) = \lambda \cdot (\omega_1^0, \omega_2^0)$  remains close to 1. Some points of the continuation are given in Table 5.

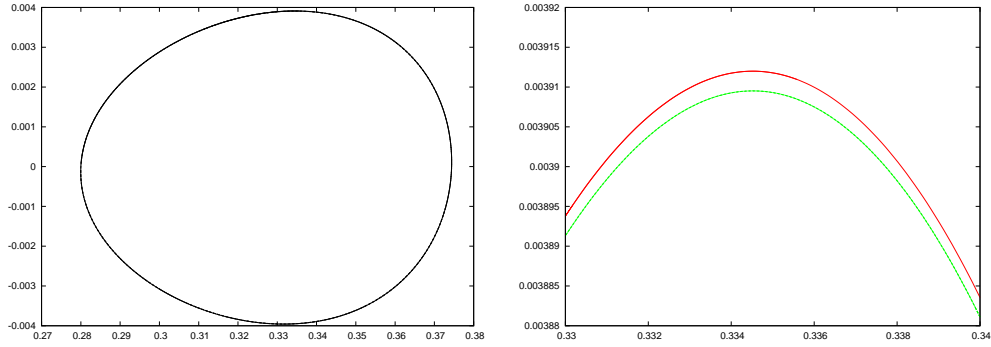


Figure 3: Left: We show initial conditions  $\alpha^0$  (horizontal axis) versus  $\rho^0$  (vertical axis) corresponding to the continuation of two families of LITs of the planar CRTBP, starting from (27) and satisfying  $\omega_1 = \omega_1^0$  and  $\omega_2 = \omega_2^0$ , respectively (see (28)). Right: Zoom of the previous figure. The red curve corresponds to  $\omega_1 = \omega_1^0$  and the green curve corresponds to  $\omega_2 = \omega_2^0$ .

$\alpha^0$	$\rho^0$	$\omega_1$	$\omega_2$	$E$
0.280192522668237	-4.746451733802e-04	1.258701184120e-02	1.586106869295e-01	-1.499615628007
0.283551429742507	-1.467835855603e-03	1.258701153345e-02	1.586106830516e-01	-1.499608162928
0.291387651385253	-2.442251747710e-03	1.258701087304e-02	1.586106747299e-01	-1.499592054697
0.312418101104665	-3.641388980651e-03	1.258700955220e-02	1.586106580907e-01	-1.499559474274
0.349860839393634	-3.620165867824e-03	1.258700942856e-02	1.586106565275e-01	-1.499556387157
0.369186023210945	-1.920472002072e-03	1.258701108022e-02	1.586106773404e-01	-1.499597121045
0.373886557767825	-5.446218663226e-04	1.258701174412e-02	1.586106857269e-01	-1.499613316143
0.373639891395473	9.059898423750e-04	1.258701170747e-02	1.586106852443e-01	-1.499612387125
0.371338111569159	1.670287803542e-03	1.258701136790e-02	1.586106809653e-01	-1.499604135924
0.364930005843379	2.685801790546e-03	1.258701056931e-02	1.586106709022e-01	-1.499584604355
0.346262823927619	3.774163590467e-03	1.258700925423e-02	1.586106543306e-01	-1.499552041160
0.337949663115750	3.901040603424e-03	1.258700905388e-02	1.586106518137e-01	-1.499547050923
0.301019986433853	2.946177436291e-03	1.258701016835e-02	1.586106658496e-01	-1.499574729371
0.281997822713248	8.833214227426e-04	1.258701167269e-02	1.586106848164e-01	-1.499611563592

Table 5: A list of initial conditions on corresponding to iso-energetic continuation of the initial condition (27) for the planar CRTBP.

331 Finally, we consider the initial conditions of two different LITs of the planar CRTBP, and we use the method of  
 332 Section 2.4 to compute some Fourier coefficients of the corresponding parameterizations. In this way, we illustrate  
 333 that we can obtain a good enough approximation of the parameterization with a reasonable computational cost. As  
 334 noted in Section 2.4, this approximate parameterization can be introduced as an initial guess for a parameterization  
 335 KAM method. Explicitly, we consider the LITs with initial conditions given by (27) and the gray row in Table 5.  
 336 In both cases the corresponding frequencies are known. Then, we take  $p_f = 7$  and  $q_f = 18$ , and we compute  $\hat{\gamma}_k$ ,  
 337  $k = (k_1, k_2)$ , for  $|k_1| + |k_2| \leq 5$ ,  $|k_1| \leq 4$ , and  $|k_2| \leq 4$ . Results are shown in Fig. 4. We show in red some  
 338 points corresponding to the numerical integration of the initial condition. In blue, we plot some curves obtained  
 339 by mapping by the approximated parameterization some circles of the form  $\theta_1 = \text{const.}$  and  $\theta_2 = \text{const.}$ . In both  
 340 cases we observe a very nice agreement between the blue and red figures.

### 341 3.2.2 The spatial case

342 If  $e = 0$ , we cannot properly speak about the stability domain of  $L_5$  in the spatial CRTBP, as the 3-dimensional  
 343 LITs of the system do not act as barriers in the 5-dimensional energy manifolds. The same happens if  $e \neq 0$ , since  
 344 we have 4-dimensional LITs in the 7-dimensional extended phase space. Hence, for a general trajectory of these  
 345 spatial problems, we can only ask for effective stability (i.e., stability for a very long time span). Nevertheless,  
 346 the domain of effective stability of the spatial CRTBP behaves similarly as the domain of perpetual stability in the  
 347 planar CRTBP. We refer to [27] for a complete frequency analysis of this domain.

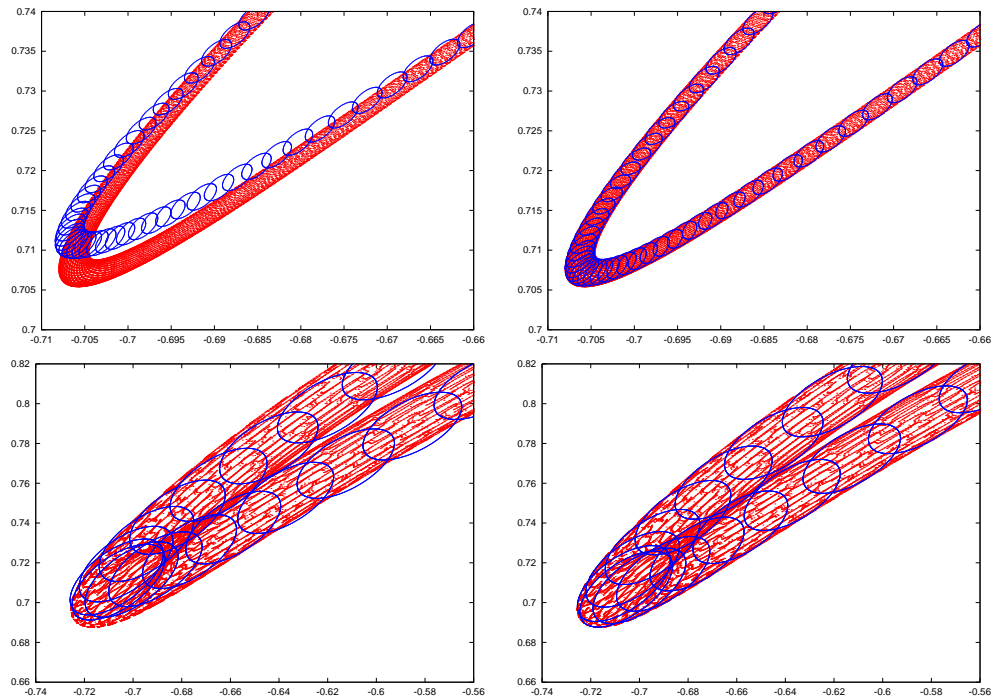


Figure 4: We compare in the plane  $xy$  the numerical integration of a trajectory on a LIT of the CRTBP with an approximate parameterization of the LIT. Top plots correspond to the LIT with initial condition (27) and bottom plots correspond to initial condition in the gray row of Table 5. Left plots correspond to the truncated parameterization defined by the Fourier coefficients of order  $k = (k_1, k_2)$  for  $|k_1| + |k_2| \leq 3$ ,  $|k_1| \leq 2$ , and  $|k_2| \leq 2$ . Right plots correspond to the Fourier coefficients for  $|k_1| + |k_2| \leq 5$ ,  $|k_1| \leq 4$ , and  $|k_2| \leq 4$ .

First, we perform the numerical continuation of 3-dimensional LITs in the spatial CRTBP. We consider the LIT of the planar CRTBP with initial condition given in (27) and frequencies  $\omega_1^0$  and  $\omega_2^0$  given in (28). If we denote by  $\mathcal{F} = (\omega_1, \omega_2, \omega_3)$  the frequency map of the spatial CRTBP, defined as function of the variables  $(\alpha, \rho, z)$ , labeling the selected initial conditions, then the equations  $\omega_1 = \omega_1^0$  and  $\omega_2 = \omega_2^0$  define a Cantor curve in the  $(\alpha, \rho, z)$ -space, that we parameterize by the arc parameter. The vertical frequency  $\omega_3$  moves along this curve, close to the initial value  $\omega_3^0 = 1$ . We ask for a tolerance of  $10^{-14}$  in the computation of the frequencies and  $10^{-10}$  in the Newton method. Results are shown in the left plot of Fig. 5. We perform similar computations starting from other four spatial LITs close to  $L_5$ , which are characterized by the following initial conditions

$$\alpha = 0.30378, \quad \rho = -0.0063897277308054, \quad z = 0.16, \quad (29)$$

$$\alpha = 0.28194, \quad \rho = -0.0127279858304461, \quad z = 0.226, \quad (30)$$

$$\alpha = 0.37788, \quad \rho = -0.0214910665205657, \quad z = 0.294, \quad (31)$$

$$\alpha = 0.20550, \quad \rho = -0.0048939829652115, \quad z = 0.14. \quad (32)$$

These LITs have “planar frequencies” given, respectively, by

$$\begin{aligned} \omega_1^0/2\pi &= 0.0126239732852498, & \omega_2^0/2\pi &= 0.158641602983746, \\ \omega_1^0/2\pi &= 0.0123864185088543, & \omega_2^0/2\pi &= 0.158640812829964, \\ \omega_1^0/2\pi &= 0.0122301409937443, & \omega_2^0/2\pi &= 0.158658687002319, \\ \omega_1^0/2\pi &= 0.0116130461983901, & \omega_2^0/2\pi &= 0.158552760666373. \end{aligned}$$

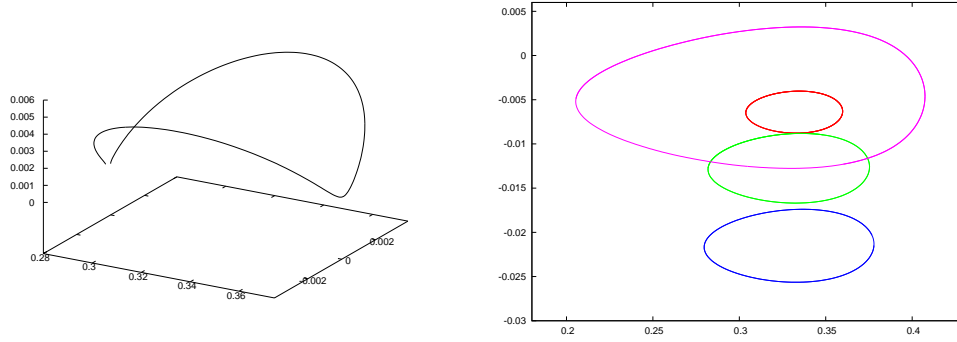


Figure 5: Numerical continuation of LITs in the spatial CRTBP defined by  $\omega_1 = \omega_1^0$  and  $\omega_2 = \omega_2^0$ , for different values of  $\omega_1^0$  and  $\omega_2^0$ . Left: We show the continuation curve in the  $(\alpha, \rho, z)$ -space, for  $z > 0$ , for the frequencies (28). Right: We show the  $(\rho, \alpha)$ -projection of the continuation curve for the initial conditions given by (29) (in red), (30) (in green), (31) (in blue), and (32) (in magenta).

348 These frequencies have been computed by frequency analysis (see [27]). The corresponding continued families of  
 349 LITs associated to the equations  $\omega_1 = \omega_1^0$  and  $\omega_2 = \omega_2^0$  are shown in the right plot of Fig. 5.

350 The final application is the numerical continuation of LITs in the (spatial) ERTBP. If we denote the frequency  
 351 map of  $H_e$  as  $\omega = (\omega_1, \omega_2, \omega_3, \omega_4)$ , then  $\omega_4$  takes the constant value  $\omega_4 = 1$ . Hence, we only need three parameters  
 352 to characterize a LIT of  $H_e$ , so we can use the variables  $(\alpha, \rho, z)$  that parameterize the selected initial conditions on  
 353 the zero velocity manifold having zero true anomaly. For any initial parameters  $(\alpha^0, \rho^0, z^0)$  labeling an invariant  
 354 torus of the spatial CRTBP (for  $e = 0$ ), with frequency vector  $(\omega_1^0, \omega_2^0, \omega_3^0)$ , we continue numerically with respect  
 355 to  $e$  the LIT that verifies  $\omega_1 = \omega_1^0$ ,  $\omega_2 = \omega_2^0$ , and  $\omega_3 = \omega_3^0$ . If the vector  $(\omega_1^0, \omega_2^0, \omega_3^0, \omega_4^0 = 1)$  is Diophantine,  
 356 then the continuation curve is continuous in the  $(\alpha, \rho, z)$ -space. We illustrate this process considering the four  
 357 initial conditions given by (29), (30), (31), and (32). The third frequency associated to these initial conditions  
 358 is given by  $\omega_3^0/2\pi = 0.159157707621790$ ,  $\omega_3^0/2\pi = 0.159162876109802$ ,  $\omega_3^0/2\pi = 0.159162723016639$ , and  
 359  $\omega_3^0/2\pi = 0.159195170134776$ , respectively. The result of this numerical continuation is shown in Fig. 6. We stop  
 360 the computations at the turning point that appears for  $\alpha \simeq 1/3$ , that is, when the LIT is situated above the point  
 361  $L_5$ . It is worth mentioning that this is not a destruction mechanism of LITs. This simply means that we cannot  
 362 expect to find LITs of a given frequency vector for arbitrary values of the eccentricity. We point out that the larger  
 363 value of the eccentricity that we obtain for the selected LITs is  $e \simeq 0.0063$ , which is far away from the actual  
 364 value of the eccentricity of the Sun-Jupiter system,  $e_{SJ} = 0.048775$ . This occurs because the values attained by  
 365 the frequency map around the point  $L_5$  change significantly when we move  $e$ . Hence, even for significantly small  
 366 values of  $e$ , we cannot expect to find a LIT of  $H_e$  with the same frequencies as for the case  $e = 0$ . For example, a  
 367 frequency analysis reveals that, for  $e = e_{SJ}$ , the frequencies around  $L_5$  are  $\omega_1 \simeq 0.0129$  and  $\omega_2 \simeq 0.15784$ .

## 368 Acknowledgements

369 We want to thank Arturo Vieiro for many discussions and comments. Some of these discussions led to interesting  
 370 ideas that will be presented in a subsequent work.

## 371 References

- 372 [1] G. Benettin, L. Galgani, and A. Giorgilli. Numerical investigations on a chain of weakly coupled rotators in  
 373 the light of classical perturbation theory. *Nuovo Cimento B (11)*, 89(2):103–119, 1985.

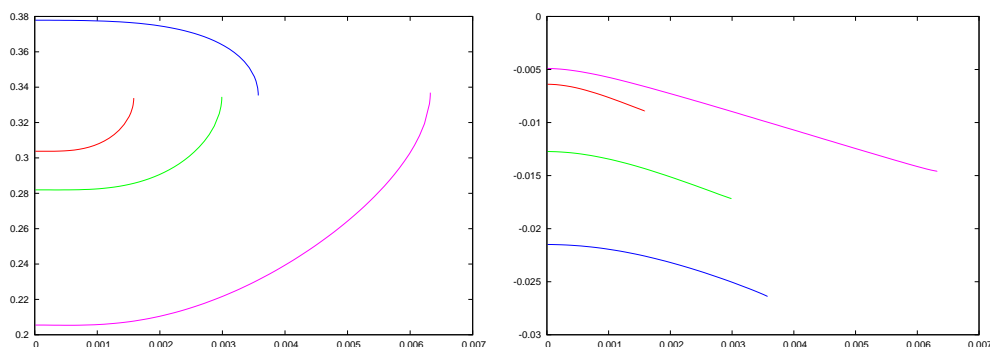


Figure 6: Numerical continuation of LIT in the spatial ERTBP with respect to  $e$ , defined by the equations  $\omega_1 = \omega_1^0$ ,  $\omega_2 = \omega_2^0$  and  $\omega_3 = \omega_3^0$ , for the values of  $\omega_1^0$ ,  $\omega_2^0$  and  $\omega_3^0$  associated to the initial conditions given by (29) (in red), (30) (in green), (31) (in blue), and (32) (in magenta). Left: We show the parameter  $\alpha$  vs  $e$ . Right: We show the parameter  $\rho$  vs  $e$ .

- 374 [2] H.W. Broer, G.B. Huitema, and M.B. Sevryuk. *Quasi-periodic motions in families of dynamical systems.*  
 375 *Order amidst chaos.* Lecture Notes in Math., Vol 1645. Springer-Verlag, Berlin, 1996.
- 376 [3] E. Castellà and À. Jorba. On the vertical families of two-dimensional tori near the triangular points of the  
 377 bicircular problem. *Celestial Mech. Dynam. Astronom.*, 76(1):35–54, 2000.
- 378 [4] A. Celletti and A. Giorgilli. On the stability of the Lagrangian points in the spatial restricted problem of three  
 379 bodies. *Celestial Mech. Dynam. Astronom.*, 50(1):31–58, 1991.
- 380 [5] B.V. Chirikov. A universal instability of many-dimensional oscillator systems. *Phys. Rep.*, 52(5):264–379,  
 381 1979.
- 382 [6] S. Das, Y. Saiki, E. Sander, and J.A. Yorke. Quantitative quasiperiodicity. Preprint available at arXiv, num:  
 383 1508.00062v1.
- 384 [7] R. de la Llave. A tutorial on KAM theory. In *Smooth ergodic theory and its applications (Seattle, WA, 1999)*,  
 385 volume 69 of *Proc. Sympos. Pure Math.*, pages 175–292. Amer. Math. Soc., Providence, RI, 2001.
- 386 [8] R. de la Llave, A. González, À. Jorba, and J. Villanueva. KAM theory without action-angle variables.  
 387 *Nonlinearity*, 18(2):855–895, 2005.
- 388 [9] L. Dieci, J. Lorenz, and R.D. Russell. Numerical calculation of invariant tori. *SIAM J. Sci. Statist. Comput.*,  
 389 12(3):607–647, 1991.
- 390 [10] E. Fermi, J. Pasta, S. Ulam, and M. Tsingou. Studies of nonlinear problems I. Technical Report LA 1940,  
 391 Los Alamos Scientific Laboratory, 1955.
- 392 [11] C. Froeschlé. Numerical study of a four-dimensional mapping. *Astronom. and Astrophys.*, 16:172–189, 1972.
- 393 [12] F. Gabern, À. Jorba, and U. Locatelli. On the construction of the Kolmogorov normal form for the Trojan  
 394 asteroids. *Nonlinearity*, 18(4):1705–1734, 2005.
- 395 [13] G. Gómez, À. Jorba, J. Masdemont, and C. Simó. *Study of Poincaré maps for orbits near Lagrangian points.*  
 396 ESA-ESOC contract 8711/91/D/IM/(SC), Darmstadt, Germany, 1993.
- 397 [14] G. Gómez, J.-M. Mondelo, and C. Simó. A collocation method for the numerical Fourier analysis of quasi-  
 398 periodic functions. I. Numerical tests and examples. *Discrete Contin. Dyn. Syst. Ser. B*, 14(1):41–74, 2010.



- 399 [15] À. Haro, M. Canadell, J.-Ll. Figueras, A. Luque, and J.M. Mondelo. The parameterization method for  
400 invariant manifolds: from theory to effective computations. Manuscript.
- 401 [16] A. Haro and R. de la Llave. New mechanisms for lack of equipartition of energy. *Phys. Rev. Lett.*, 85(9):1859–  
402 1862, 2000.
- 403 [17] M. Huang, T. Küpper, and N. Masbaum. Computation of invariant tori by the Fourier methods. *SIAM J. Sci.*  
404 *Comput.*, 18(3):918–942, 1997.
- 405 [18] G. Huguet, R. de la Llave, and Y. Sire. Computation of whiskered invariant tori and their associated mani-  
406 folds: new fast algorithms. *Discrete Contin. Dyn. Syst.*, 32(4):1309–1353, 2012.
- 407 [19] À. Jorba and J. Villanueva. On the normal behaviour of partially elliptic lower-dimensional tori of Hamilto-  
408 nian systems. *Nonlinearity*, 10(4):783–822, 1997.
- 409 [20] À. Jorba and J. Villanueva. On the persistence of lower-dimensional invariant tori under quasi-periodic  
410 perturbations. *J. Nonlinear Sci.*, 7(5):427–473, 1997.
- 411 [21] À. Jorba and J. Villanueva. Numerical computation of normal forms around some periodic orbits of the  
412 restricted three-body problem. *Phys. D*, 114(3-4):197–229, 1998.
- 413 [22] Chr. Kaas-Petersen. Computation, continuation, and bifurcation of torus solutions for dissipative maps and  
414 ordinary differential equations. *Phys. D*, 25(1-3):288–306, 1987.
- 415 [23] J. Laskar. The chaotic motion of the solar system. A numerical estimate of the size of the chaotic zones.  
416 *Icarus*, 88:266–291, 1990.
- 417 [24] A Luque and A. Vieiro. Jet transport in frequency analysis. In preparation.
- 418 [25] A. Luque and J. Villanueva. Computation of derivatives of the rotation number for parametric families of  
419 circle diffeomorphisms. *Phys. D*, 237(20):2599–2615, 2008.
- 420 [26] A. Luque and J Villanueva. Numerical computation of rotation numbers for quasi-periodic planar curves.  
421 *Phys. D*, 238(20):2025–2044, 2009.
- 422 [27] A. Luque and J. Villanueva. Quasi-periodic frequency analysis using averaging-extrapolation methods. *SIAM*  
423 *J. Appl. Dyn. Syst.*, 13(1):1–46, 2014.
- 424 [28] F. Schilder, H.M. Osinga, and W. Vogt. Continuation of quasi-periodic invariant tori. *SIAM J. Appl. Dyn.*  
425 *Syst.*, 4(3):459–488 (electronic), 2005.
- 426 [29] F. Schilder, H.M. Osinga, and W. Vogt. Fourier methods for quasi-periodic oscillations. *Internat. J. Numer.*  
427 *Methods Engrg.*, 67(5):629–671, 2006.
- 428 [30] T.M. Seara and J. Villanueva. On the numerical computation of Diophantine rotation numbers of analytic  
429 circle maps. *Phys. D*, 217(2):107–120, 2006.
- 430 [31] C. Simó. Effective computations in celestial mechanics and astrodynamics. In *Modern methods of analytical*  
431 *mechanics and their applications (Udine, 1997)*, pages 55–102. Springer, Vienna, 1998.
- 432 [32] V. Szebehely. *Theory of Orbits - The Restricted Problem of Three Bodies*. Academic Press, New York, 1967.